Laser-Doppler flowmetry at large interoptode spacing in human tibia diaphysis: Monte Carlo simulations and preliminary experimental results

2011 Physiol. Meas. 32 N33

(http://iopscience.iop.org/0967-3334/32/11/N01)

Physiol. Meas. **32** (2011) N33–N53 doi:10.1088/0967-3334/32/11/N01

NOTE

Laser-Doppler flowmetry at large interoptode spacing in human tibia diaphysis: Monte Carlo simulations and preliminary experimental results

Tiziano Binzoni[1,2], David Boggett[3] and Dimitri Van De Ville[2,4]

[1] Département des Neurosciences Fondamentales, University of Geneva, Switzerland
[2] Département de l'Imagerie et des Sciences de l'Information Médicale, University Hospital, Geneva, Switzerland
[3] Moor Instruments Ltd, Millwey, Axminster, UK
[4] Institute of Bioengineering, Ecole Polytechnique Fédérale de Lausanne (EPFL), Switzerland

E-mail: tiziano.binzoni@unige.ch

Received 9 June 2011, accepted for publication 22 September 2011
Published 26 October 2011
Online at stacks.iop.org/PM/32/N33

Abstract
Laser-Doppler flowmetry (LDF) is an outstanding tool to monitor blood flow in a continuous and non-invasive way. In this work, we study LDF at large interoptode spacing applied to a human bone model (i.e. tibia diaphysis). To that aim, we first performed an extensive set of Monte Carlo (MC) simulations for 10 and 25 mm interoptode spacing. Second, we have assembled a dedicated LDF instrumentation based on an optimized industrial avalanche photo-detector. We performed LDF experimental measurements on human muscle using well-known physiological protocols, which confirmed the reliability of our instrumentation and the relevance of the LDF algorithms tested with the MC simulations. In a second set, we repeated the measurements on human tibia diaphysis. Again, the experiments corroborate the MC simulations and demonstrate the effectiveness of LDF to monitor blood perfusion in bone. The proposed technique has great potential for non-invasive neuro-vascular studies since it will certainly help to reveal the mechanisms underlying the interaction between bone/bone marrow, the circulatory system and the nervous system.

(Some figures in this article are in colour only in the electronic version)

1. Introduction

The circulatory system in bone is not merely a passive conduit for blood but it plays an important role in controlling the physiological processes (McCarthy 2006). The high plasticity of the vascular tree allows it to adapt its geometry to the physiological needs, e.g. during human growth and ageing or in pathological conditions (Brookes and Revell 1998). Blood vessels in bone do not only transport substrates useful for energy metabolism or osteogenesis, but

they may have an active role in skeletal homeostasis (McCarthy 2006). Bone blood flow by itself may excite different pathways related to bone growth and remodelling by directly stimulating specialized bone cells (Klein-Nulend *et al* 2005). Bone is an extraordinarily vital tissue possessing a rich innervation that participates for example not only in the control of the blood flow (Brookes and Revell 1998) but probably also in the regulation of bone metabolism (Chenu 2001). A sensitive innervation is also present (McCarthy 2006).

In this context, better understanding the mechanisms underlying the interaction between bone, the circulatory system and the nervous system appears to be a fundamental point. In particular, the potential clinical impact of this knowledge encourage us to perform these investigations directly in humans. Thus, a non-invasive technique allowing the continuous assessment of blood flow or speed in human bone/bone marrow is certainly a first useful step in this sense. In fact, the nature of the bone itself renders it exceptionally difficult to investigate the circulation. Measurement techniques that are usually applied in laboratory are difficult or impossible to apply on humans, and when applicable they are partially invasive and allow only few measurements in time (Brookes and Revell 1998).

For these reasons, some years ago our group investigated the possibility of exploiting near-infrared spectroscopy to assess non-invasively parameters linked to blood perfusion and blood volume in human bone (Binzoni *et al* 2002, 2003a, 2006). It has been possible to show that near-infrared light can access bone cortex or bone marrow (human tibia diaphysis). This allowed us to observe for example that the reoxygenation rate, after a 3 min ischaemic period, is slower in tibia bone marrow than in skeletal muscle (*tibialis anterior*) and that it decreases with increasing age (age range 25–75 years) in muscle, but that it remains constant in bone marrow (Binzoni *et al* 2003a). In the same work, it has also been shown that blood oxygen saturation is higher in bone marrow and it remains constant as a function of age while it decreases is muscle. In another study, it was found that the vascular volume (tibia bone/bone marrow) increases when the subject is submitted to an orthostatic stress (tilt bed) and that an arterio-venous reflex might be present during the tilt as it normally happens in skeletal muscle (Binzoni *et al* 2006). On the other hand, Näslund *et al* (2006) have shown by photoplethysmography (using near-infrared wavelength) that it is possible to observe blood pulsations in human patellar trabecular bone.

Thus, apart from the physiological interest, the cited series of works states that near-infrared light appears to be a probe of choice allowing us to investigate human bone/bone marrow non-invasively. On the other hand, it is also clear that measurement techniques more directly linked to blood flow or speed need to be developed. For this reason, in the present contribution we propose the use of laser-Doppler flowmetry (LDF; near-infrared laser) at large interoptode spacing as a non-invasive tool allowing the monitoring of bone/bone marrow blood flow changes in the human tibia. Both Monte Carlo simulations and preliminary experimental results demonstrate that LDF at large interoptode spacing shows a slightly different behaviour compared to 'classical' LDF at short interoptode spacing. Considering the unique characteristics of the method described in this note, we hope that it will lead to original investigations of the physiology, pathophysiology and pharmacology of the neuro-vascular system in human bone/bone marrow.

2. Material and methods

2.1. Laser-Doppler flowmeter

Based on previous work (Binzoni *et al* 2003), an improved customized laser-Doppler flowmeter, allowing work at large interoptode spacing (r), has been assembled to test the

feasibility of the measurements on human tibia diaphysis. The laser-Doppler flowmeter consisted of a 785 nm laser source (IRLD50, Moor Instruments Ltd., UK) and a custom-made avalanche photo-detector (APD) module (Hamamatsu, Japan) with an active detection area of 1.5 mm diameter and a photoelectric sensitivity at 800 nm of 2.1×10^8 V W^{-1} (minimum detection limit 47 pW rms). The cutoff frequencies of the APD module (anti-alias filter) were 0 and 75 kHz (−3 dB). A 1.5 m multimode optical fibre (core diameter 400 μm), with a cylindric acetal probe head at the tissue/fibre interface, was connected to the laser. This gave a total of 45 mW of light at the probe head. A 1.5 m detection fibre (core 140 or 200 μm depending on the needs) was connected to the APD module with an identical probe head as for the source fibre. All the probes were custom made (Moor Instruments Ltd., UK). The signal (voltage), representing the photo-electric current ($i(t)$) as a function of time (t), was directly acquired from the APD module output by using an analogue-to-digital acquisition card (NI USB-6251, National Instruments Corporation, Hungary). The ADC resolution was 16 bits and the input range was set to ±5 V. The dc component of the measured laser-Doppler signals was always in the interval [0, 5] V. The ac modulation for the smallest signals was of the order of 10 mV, thus detectable by the ADC card. The sampling frequency was set to 1 MHz in order to cover all frequencies (ν) observed at the APD module output and to eliminate the possibility of generating aliases that may affect the wanted LDF signals (see section 4). The number of sampled points was $2^{17} = 131\,072$. The acquisition card was connected to a portable PC through a USB connection. The acquisition software and data treatment was written in MATLAB® language (The Mathworks Inc., Natick, MA, USA).

2.2. *Monte carlo simulations:* $\langle\omega^0\rangle$ *and* $\langle\omega^1\rangle$

In classical LDF ($r < 1$ mm), the zero- ($\langle\omega^0\rangle$) and first-order ($\langle\omega^1\rangle$) moments,

$$\langle\omega^n\rangle := \int_{-\infty}^{\infty} |\omega|^n \, P(\omega) \, \mathrm{d}\omega, \tag{1}$$

($n \in \{0, 1\}$) of the power spectrum of $i(t)$,

$$P(\omega) := \left| \int_{-\infty}^{\infty} i(t) \, \mathrm{e}^{-\mathrm{i}\omega t} \, \mathrm{d}t \right|^2, \tag{2}$$

($\omega = 2\pi\nu$ is the angular frequency) normalized by the square of the mean photo-electric current,

$$i_0 := \lim_{T \to +\infty} \frac{1}{2T} \int_{-T}^{T} i(t) \, \mathrm{d}t, \tag{3}$$

are considered proportional to the tissue blood volume and blood flow (perfusion), respectively (Bonner and Nossal 1981). To investigate whether this rule still holds at large r ($r \geqslant 10$ mm), we have performed Monte Carlo simulations. The method is well known and the approach utilized has been previously published (Binzoni *et al* 2009). In summary, the virtual tissue phantom was represented by a semi-infinite medium, which is the geometry for which the behaviour of $\langle\omega^0\rangle / i_0^2$ and $\langle\omega^1\rangle / i_0^2$ is usually investigated (Bonner and Nossal 1981). The LDF was represented as a point-source/detector configuration, with the source normal to the plane. The simulations reported in this note required in total 773 h computation time on an eight-node cluster; each single simulation was performed by running 10^7 photon packets.

To explain the complex behaviour of an LDF at large interoptode spacing, two different experimental conditions have been taken into account. The first one represents a situation where the blood can flow inside the vascular tree. A venous occlusion is included in this condition because the blood can circulate even if the resistance to the flow is increased.

To simplify we will call this condition 'free-flow'. The second condition is well described by an arterial occlusion. In this case, the blood cannot circulate inside the vessels and the only allowed displacement of the erythrocytes is a limited random movement without net displacement. We will name this condition 'stopped-flow'. In fact, we will see that from the LDF point-of-view these are very different situations that lead to different interpretations of the LDF data.

2.2.1. Free-flow. Three batches of Monte Carlo simulations, corresponding to r equal to 0.5 (classical LDF), 10 and 25 mm, were performed. To take into account a large number of physiological conditions, the erythrocytes' velocity was modelized with a normal distribution (root mean square velocity $\langle V^2_{\text{Brown}}\rangle^{1/2}$) plus the possibility of having a bulk movement ($\vec{V}_{\text{trans}}$) (Binzoni *et al* 2004). For a given r, the optical and physiological parameters where chosen as all the combinations of the following values: $\langle V^2_{\text{Brown}}\rangle^{1/2} \in \{0.5, 1, 2, 3\}$ mm s^{-1}, $\|\vec{V}_{\text{trans}}\| \in \{0, 0.5, 1, 2\}$ mm s^{-1} (where $\vec{V}_{\text{trans}}$ is parallel to the plane), $\mu'_{\text{s}} \in \{0.4, 0.6, 0.8\}$ mm^{-1} (reduced scattering coefficient), $\mu_{\text{a}} \in \{0.015, 0.02, 0.025\}$ mm^{-1} (absorption coefficient), $n = 1.4$ (refractive index), $g = 0.9$ (anisotropy parameter). When a photon interacts with a scatterer inside the tissue, the probability, P_{move}, that it is a moving scatterer (erythrocyte) is estimated as (Kienle 2001)

$$P_{\text{move}} \approx c_b \frac{\mu_{\text{s,blood}}}{\mu_{\text{s}}} \approx 1.68 \frac{\mu_{\text{a}}}{\mu'_{\text{s}}}, \tag{4}$$

where c_b is the concentration of the blood (i.e. the volume of blood per unit volume of tissue), $\mu_{\text{s,blood}}$ is the scattering coefficient of the blood and μ_{s} is the scattering coefficient of the considered tissue, blood included. The parameters $\mu_{\text{s,blood}}$ and μ_{s} can be also seen as the probability per unit length that a photon will be scattered by an erythrocyte (in blood only) and the probability per unit length that a photon will be scattered by any scatterer (moving and not moving) in the whole tissue. By weighting $\mu_{\text{s,blood}}$ and μ_{s} by the respective tissue volume fractions, i.e. c_b and 1, one obtains equation (4). The equation has then been expressed in term of the simulation parameters μ_{a} and μ'_{s}. The parameter c_b is now implicitly expressed through μ_{a}. The factor 1.68 allows us to 'calibrate' equation (4) to obtain $P_{\text{move}} = 0.07$ when $\mu_{\text{a}} = 0.025$ mm^{-1} and $\mu'_{\text{s}} = 0.6$ mm^{-1}, corresponding to a reasonable value for skeletal muscle. The P_{move} values for other physiological conditions or tissues are automatically computed by varying μ_{a} and μ'_{s}. For a given tissue, the parameter μ'_{s} can be considered as a reasonable approximation to remain constant when varying blood volume (related to μ_{a}). In this manner, we generate a sufficient number of P_{move}, optical and physiological parameters for the simulations, covering a large range of combinations. In the Monte Carlo simulations, each combination of these parameters leads to a triplet of $\langle\omega^0\rangle$, $\langle\omega^1\rangle$ and i_0 values, for a given r. For the sake of completeness, we note that other potential scatterers than erythrocytes are present in blood, such as, for example, leukocytes or platelets. However, these scatterers represent only 1% of the total blood volume, compared to erythrocytes that roughly represent 42–48%. In this sense, moving red blood cells represent the main contribution to the scattering process. For this reason, in the present context we make the commonly accepted hypothesis that only red blood cells contribute to the laser-Doppler effect.

The mean velocity, $\langle\|\vec{V}\|\rangle$, of the erythrocytes can be computed as usual as (e.g. equation (14) in Binzoni and Van De Ville 2008)

$$\langle\|\vec{V}\|\rangle = \frac{\sqrt{6}}{3}\frac{\langle V^2_{\text{Brown}}\rangle^{1/2}}{\sqrt{\pi}} \text{e}^{-\frac{3}{2}\frac{\|\vec{V}_{\text{trans}}\|^2}{\langle V^2_{\text{Brown}}\rangle}} \left(\|\vec{V}_{\text{trans}}\| + \frac{\langle V^2_{\text{Brown}}\rangle^{1/2}}{3\|\vec{V}_{\text{trans}}\|}\right) \text{erf}\left(\frac{\sqrt{6}}{2}\frac{\|\vec{V}_{\text{trans}}\|}{\langle V^2_{\text{Brown}}\rangle^{1/2}}\right). \tag{5}$$

In practice, in classical LDF, $\langle\omega^0\rangle/i_0^2$ is considered to be proportional to P_{move} (related to blood volume) and $\langle\omega^1\rangle/i_0^2$ proportional to $P_{\text{move}}\langle\|\vec{V}\|\rangle$ (related to blood flow). To our knowledge, it is not perfectly clear if this relationship still holds in all conditions at large interoptode spacing. The Monte Carlo simulations should bring some insight on this point.

2.2.2. Stopped-flow. We have seen in the previous section (equation (4)) that in the 'free-flow' condition the fraction of moving erythrocytes, P_{move}, is related to their concentration, c_b, through the coefficient μ_a. However, in some special conditions, such as during an arterial occlusion, this relationship does not hold anymore. In this case, before and after occlusion we may have the same μ_a (i.e. same total number of erythrocytes), but after occlusion the fraction of moving erythrocytes is strongly decreased. Intuitively, the majority of erythrocytes does not move at all and the remaining ones undergo a slow Brownian movement with no net displacement ($\|\vec{V}_{\text{trans}}\| = 0$). In this case, equation (4) gives the same P_{move}, but we know that its value must be strongly decreased. For this reason, to take into account this possibility, a series of simulations have been performed by fixing to a small value: $P_{\text{move}} = 0.001$ and $\|\vec{V}_{\text{trans}}\| = 0$. The remaining parameters being the same as in the previous section and with all the combinations of r, $\left\langle V_{\text{Brown}}^2\right\rangle^{1/2}$, μ_s' and μ_a values as above.

2.3. Experimental LDF tests

To practically present the experimental LDF setup and to show how to interpret the measurements based on the Monte Carlo simulations preliminary experiments were performed on one subject (one of the authors). Two different tissues were investigated: the forearm muscles and the tibia diaphysis. The skeletal muscle, being a well-known tissue from the vascular point of view, is ideal for explanatory purposes. The measurements on the human tibia demonstrate the feasibility of the proposed model and the specific behaviour of this tissue.

2.3.1. Venous occlusion: forearm. The subject was comfortably seated on a chair with the right forearm laying on a plane (hand in prone position) situated at the heart level and containing the optodes. The optodes were aligned along the direction of the radius ($r = 10$ mm) and situated symmetrically on the position where the forearm has the largest diameter. A standard pressure cuff was placed around the arm, just above the elbow.

The power spectra were acquired continuously during the experiments and one power spectrum consisted of a mean of 100 power spectra to improve the signal to noise. We also corrected the power spectrum for the 'baseline' as explained in detail in section 4.1.1. This allowed a triplet of $\langle\omega^0\rangle$, $\langle\omega^1\rangle$ and i_0 values every 29 s.

The experimental protocol consisted on a reference measurement and then three venous occlusions/reperfusion cycles of 2×3 min each (see section 3). During the occlusion periods the cuff was inflated at 50 mmHg.

2.3.2. Arterial occlusion: forearm. This protocol was the same as in section 2.3.1, but in this case the cuff was inflated at 170 mmHg during the occlusion periods.

2.3.3. Venous occlusion: tibia. This protocol was repeated two times, one for $r = 10$ mm and one for $r = 25$ mm. For these experiments the subject was seated with the feet slightly heightened to improve the comfort of the subject and to facilitate the placement of a dedicated pressure cuff. The optodes were firmly positioned on the medial surface of the tibia (diaphysis) at the half distance between the *malleolus medialis* and the *condylus medialis tibiae* (figure 1).

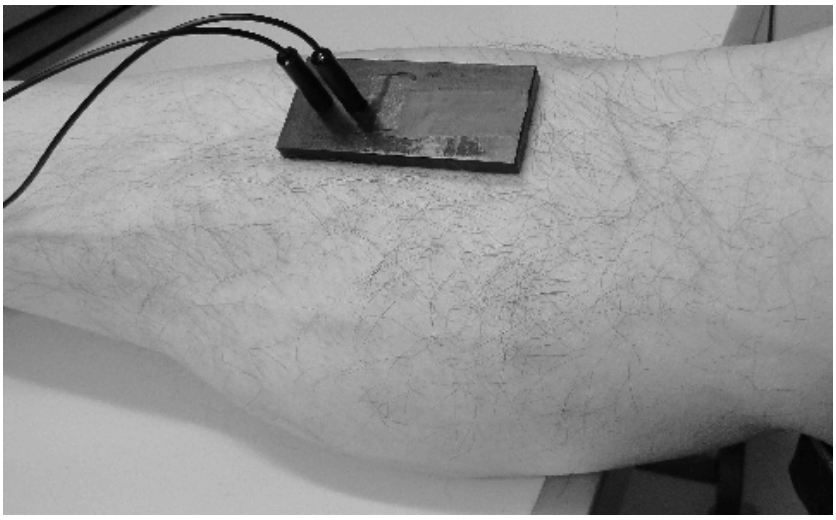

Figure 1. Optode position on the tibia. To allow the visibility of the optodes, the optode fixation system and the protective cover for unwanted light are not shown.

The pressure cuff was placed around the thigh and connected to the laboratory compressed air outlet to reach the necessary high pressure. The same occlusion/reperfusion protocol as in section 2.3.1 was applied but here the cuff was inflated at 60 mmHg during the occlusion periods.

2.3.4. Arterial occlusion: tibia. This protocol was the same as in section 2.3.3, but in this case the cuff was inflated at 250 mmHg during the occlusion periods. The higher pressure value compared to that utilized for the forearm has been chosen by following the recommendations of clinical practice (see, e.g., Tuncali *et al* 2006).

3. Results

3.1. Monte Carlo simulations

In figures 2–5 the results of the Monte Carlo simulations are reported. These figures allow the comparison of the behaviour of a classical LDF (panels a) with an LDF at large interoptode spacing (panels b and c).

In figure 2, $\langle\omega^1\rangle/i_0^2$ is shown as a function of $P_{\text{move}}\langle\|\vec{V}\|\rangle$ for r equal to 0.5, 10 and 25 mm, respectively. It is possible to observe that when r becomes large, the sensitivity to μ_s' becomes more manifest and the spread out of the points increases for increasing $P_{\text{move}}\langle\|\vec{V}\|\rangle$ values. However, for a given μ_s', the linearity is always well conserved. The points for the special case (markers with a green edge) where very few scatterers (erythrocytes) are moving, and thus contributing for a very low 'blood flow', nicely fall at the origin (it is maybe useful to remind here that LDF can 'see' only moving erythrocytes). Thus, concerning $\langle\omega^1\rangle/i_0^2$, LDF at $r \geqslant 10$ mm has a very similar behaviour to that of classical LDF.

In figure 3, $\langle\omega^1\rangle/\langle\omega^0\rangle$ is shown as a function of $\langle\|\vec{V}\|\rangle$ for r equal to 0.5, 10 and 25 mm, respectively. It is evident that in this case the normalization by $\langle\omega^0\rangle$ has the positive effect to completely eliminate the influence of μ_s' for any r. However, the particular simulation points computed for $P_{\text{move}} = 0.001$ are as expected only for classical LDF (panel a). It can be

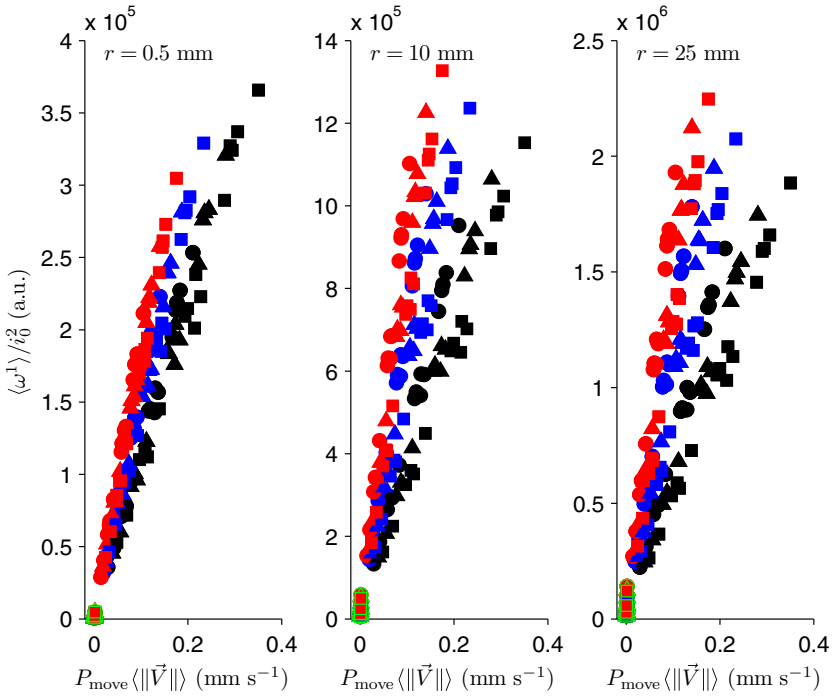

Figure 2. Monte Carlo simulation for three different interoptode distances (r). First-moment, $\langle\omega^1\rangle$, of the power spectrum of photo-electric current normalized by its squared mean, i_0, as a function of the probability, P_{move}, for a photon to interact with a moving scatterer (erythrocyte) times the mean speed of the moving scatterers (erythrocytes), $\langle\|\vec{V}\|\rangle$. The quantities $\langle\omega^1\rangle/i_0^2$ and $P_{\text{move}}\langle\|\vec{V}\|\rangle$ are interpreted as the tissue 'blood flow' (perfusion). The black, blue and red colours correspond to a μ_s' of 0.4, 0.6 and 0.8 mm^{-1}, respectively. The circle, triangle and square markers correspond to a μ_a of 0.015, 0.02 and 0.025 mm^{-1}, respectively. The markers with the green edge are the points with the special value $P_{\text{move}} = 0.001$. The ordinate units are the same for the three panels.

deduced from panels b and c that we experimentally expect an underestimation of the speed for this case (markers with green edge) when $r \geqslant 10$ mm.

In figure 4, $\langle\omega^0\rangle/i_0^2$ is shown as a function of P_{move} for r equal to 0.5, 10 and 25 mm, respectively. For $r = 0.5$ mm, $\langle\omega^0\rangle/i_0^2$ increases as expected as a function of P_{move}, whereas for $r \geqslant 10$ mm the sensitivity of $\langle\omega^0\rangle/i_0^2$ to P_{move} becomes very low. Actually, if one zooms the points with a $\langle\omega^0\rangle/i_0^2$ value around 30 au for $r = 10$ mm and $r = 25$ mm, we would observe exactly the same behaviour as in panel for $r = 0.5$ mm (not shown), but with a total variation of the order of only a fraction of one arbitrary unit. This decrease in sensitivity of the signal with increasing P_{move} at large r was previously hypothesized theoretically by Bonner and Nossal (1981). Concerning the special points (markers with green edges) computed for $P_{\text{move}} = 0.001$, we can see that $\langle\omega^0\rangle/i_0^2$ reach the lowest values for all r. In conclusion, we experimentally expect to see only a very small variation of $\langle\omega^0\rangle/i_0^2$ with changing P_{move} when $r \geqslant 10$ mm.

It is interesting to observe the behaviour of $\langle\omega^0\rangle$ when it is not normalized by i_0^2. In figure 5, $\langle\omega^0\rangle$ is shown as a function of P_{move} for r equal to 0.5, 10 and 25 mm, respectively. The parameter $\langle\omega^0\rangle$ for $r = 0.5$ behaves as expected, this time with the explicit influence

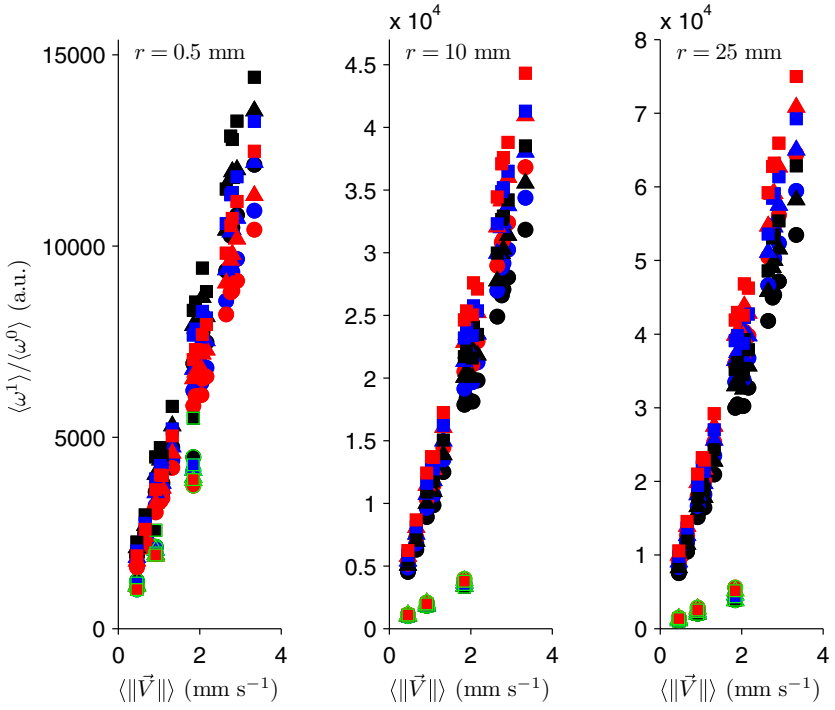

Figure 3. Monte Carlo simulation for three different interoptode distances (r). First-moment, $\langle\omega^1\rangle$, of the power spectrum of the photo-electric current normalized by the respective zero-moment, $\langle\omega^0\rangle$, as a function of the mean speed of the moving scatterers (erythrocytes), $\langle\|\vec{V}\|\rangle$. The quantities $\langle\omega^1\rangle/\langle\omega^0\rangle$ and $\langle\|\vec{V}\|\rangle$ are interpreted as the mean speed of the erythrocytes (in short 'blood speed'). The black, blue and red colours correspond to a μ_s' of 0.4, 0.6 and 0.8 mm^{-1}, respectively. The circle, triangle and square markers correspond to a μ_a of 0.015, 0.02 and 0.025 mm^{-1}, respectively. The markers with the green edge are the points with the special value $P_{move} = 0.001$. The ordinate units are the same for the three panels.

of μ_s' due to the lack of normalization by i_0^2. However, if $r \geqslant 10$ mm, then $\langle\omega^0\rangle$ displays a surprising behaviour and decreases for increasing P_{move}. Even if the influence of μ_s' is large, the advantage of this behaviour is the high sensitivity of $\langle\omega^0\rangle$ to P_{move} and with the suitable calibration it might help to detect small P_{move} changes and help for example to confirm the possible observed small variations in $\langle\omega^0\rangle/i_0^2$. It remains to be verified if this phenomenon can actually be observed experimentally (see below). Concerning the points computed with the particular $P_{move} = 0.001$ value, one could expect a large increase of $\langle\omega^0\rangle$ at $P_{move} = 0.001$ to be coherent with the negative slopes displayed by the points in panels b and c. However, as $\langle\omega^0\rangle/i_0^2$ indicates in figure 4, $\langle\omega^0\rangle$ also decreases in this case making the behaviour of $\langle\omega^0\rangle$ even more complex. Therefore, we must verify experimentally that this really happens (see below).

3.2. Experimental LDF tests: forearm

Figures 6 and 7 refer to measurements performed on skeletal muscle (forearm) and aim at checking whether LDF at $r = 10$ mm can detect the expected physiological behaviour during the different experimental tests.

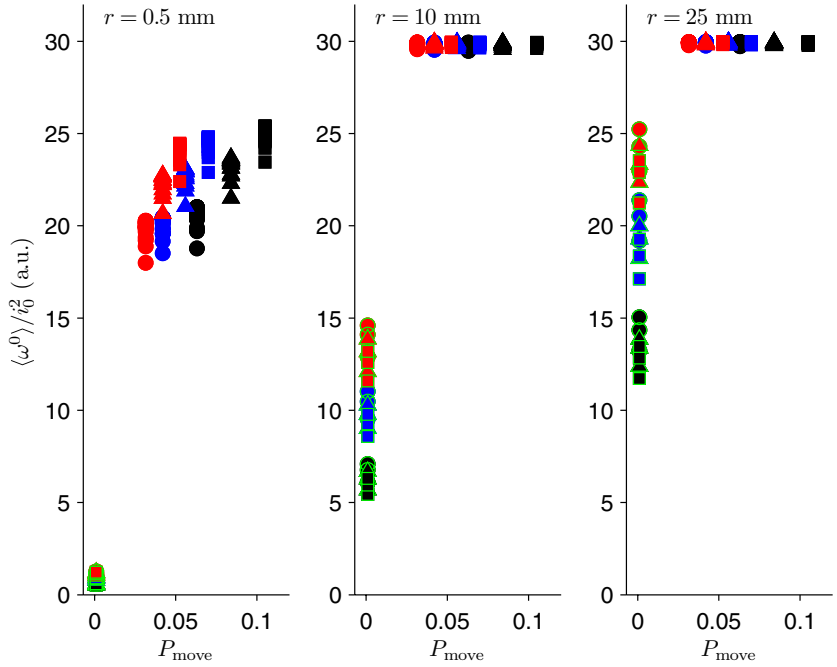

Figure 4. Monte Carlo simulation for three different interoptode distances (r). Zero-moment, $\langle\omega^0\rangle$, of the power spectrum of the photo-electric current normalized by its squared mean, i_0, as a function of the probability, P_{move}, for a photon to interact with a moving scatterer (erythrocyte). The quantities $\langle\omega^0\rangle/i_0^2$ and P_{move} are interpreted as the tissue 'blood volume'. The black, blue and red colours correspond to a μ_s' of 0.4, 0.6 and 0.8 mm^{-1}, respectively. The circle, triangle and square markers correspond to a μ_a of 0.015, 0.02 and 0.025 mm^{-1}, respectively. A zoom of the points with $P_{\text{move}} > 0.001$ represented in the panels $r = 10$ and $r = 25$ mm gives exactly the same trend as in panel $r = 0.5$ mm (i.e. a $\langle\omega^0\rangle/i_0^2$ increase for a P_{move} increase; not shown). The markers with the green edge are the points with the special value $P_{\text{move}} = 0.001$. The ordinate units are the same for the three panels.

The data reported in figure 6 are the result of a well-known plethysmographic manoeuvre (venous occlusion) introduced for the first time in near-infrared spectroscopy studies by De Blasi *et al* (1994). This is used to produce periodic increases and decreases (release of the occlusion) in tissue blood volume and thus induces relative tissue blood perfusion changes. Inflating the pressure cuff at 50 mmHg has the effect to increase tissue blood speed (figure 6(a)) and tissue blood perfusion (figure 6(b)); this is probably facilitated by the local increase in tissue blood volume. The increment in $\langle\omega^0\rangle/i_0^2$ (figure 6(c)) can be detected by the LDF at $r = 10$ mm even if this parameter is less sensitive to tissue blood volume changes at large interoptode spacing, as shown by our Monte Carlo simulations (figure 4). It is interesting to note that the non-normalized $\langle\omega^0\rangle$ (figure 6(e)) does indeed behave exactly as predicted by the Monte Carlo simulations ('free-flow') in figure 5, i.e. $\langle\omega^0\rangle$ decreases for increasing tissue blood volume. In this sense, considering the linear relationships existing between the couples of parameters (P_{move}, $\langle\omega^0\rangle/i_0^2$) and ($P_{\text{move}}$, $\langle\omega^0\rangle$), figure 6(c) is expected to be the mirror image of figure 6(e), and this seems to be the case. A small deviation to this rule is observed at the very beginning of the protocol where the initial change of $\langle\omega^0\rangle/i_0^2$ is proportionally larger than the one for $\langle\omega^0\rangle$ (see section 4). In figure 6(d), the mean intensity of the photo-electric current, i_0, is also shown. The parameter i_0 is also related to the tissue blood volume because

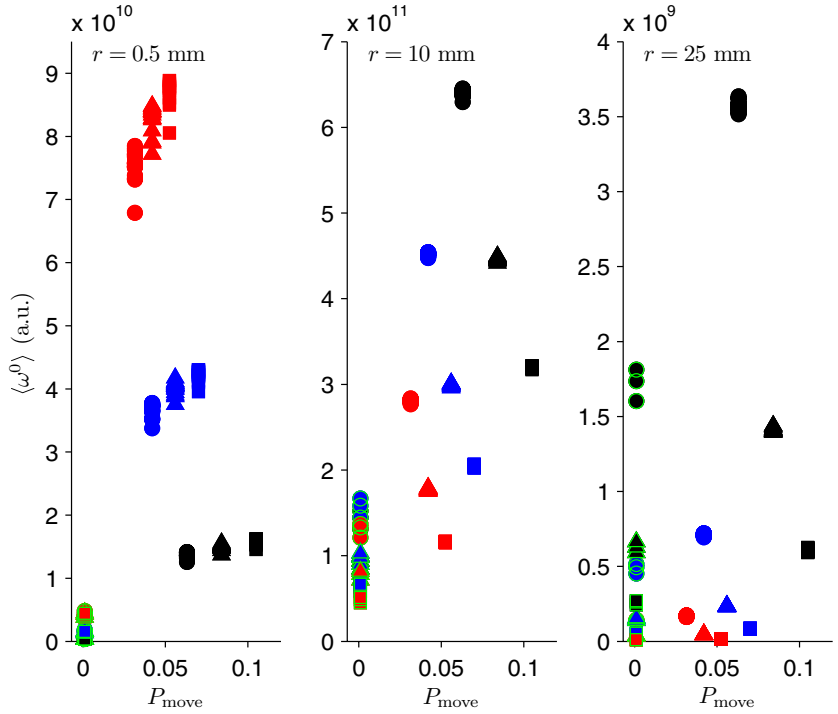

Figure 5. Monte Carlo simulation for three different interoptode distances (r). Zero-moment, $\langle\omega^0\rangle$, of the power spectrum of the photo-electric current not normalized by its squared mean, i_0, as a function of the probability, P_{move}, for a photon to interact with a moving scatterer (erythrocyte). The quantity P_{move} is interpreted as the tissue 'blood volume', while $\langle\omega^0\rangle$ as the 'un-normalized' tissue 'blood volume'. The black, blue and red colours correspond to a μ_s' of 0.4, 0.6 and 0.8 mm^{-1}, respectively. The circle, triangle and square markers correspond to a μ_a of 0.015, 0.02 and 0.025 mm^{-1}, respectively. The markers with the green edge are the points with the special value $P_{\text{move}} = 0.001$. The ordinate units are the same for the three panels.

an increase in blood concentration increases by definition μ_a and as a consequence induces a decrease in i_0 (intuitively, less photons reach the detector due to absorption). This further confirms the expected volume changes.

The protocol utilized to obtain the data presented in figure 7 had the aim to periodically stop the tissue blood perfusion and thus to experimentally create a condition analogous to the special $P_{\text{move}} = 0.001$ case of the Monte Carlo simulations ('stopped-flow'). In figure 7, the influence of the repeated arterial occlusions on the LDF parameters at $r = 10$ mm can be observed. Figure 7(a) displays the behaviour of the mean tissue blood speed, $\langle\omega^1\rangle/\langle\omega^0\rangle$, as a function of time. As expected, during each arterial occlusion interval there is a decrease in tissue blood speed and then a sudden increase when the pressure cuff is relaxed. Figure 7(b) shows the related tissue blood perfusion, $\langle\omega^1\rangle/i_0^2$, where the well-known post-occlusion reactive hyperaemia clearly appears. In figures 7(c)–(e), the parameters related to the tissue blood volume are shown as a function of time. The parameter $\langle\omega^0\rangle/i_0^2$ decreases during the occlusion, and also in this case the behaviour is compatible with the Monte Carlo simulations (markers with green edge) reported in figure 4. Interestingly enough, the behaviour of i_0 displayed in figure 7(a) reflects an increase in blood volume during arterial occlusion (see above for an explanation). The comparison between $\langle\omega^0\rangle/i_0^2$ and i_0 during the ischaemic

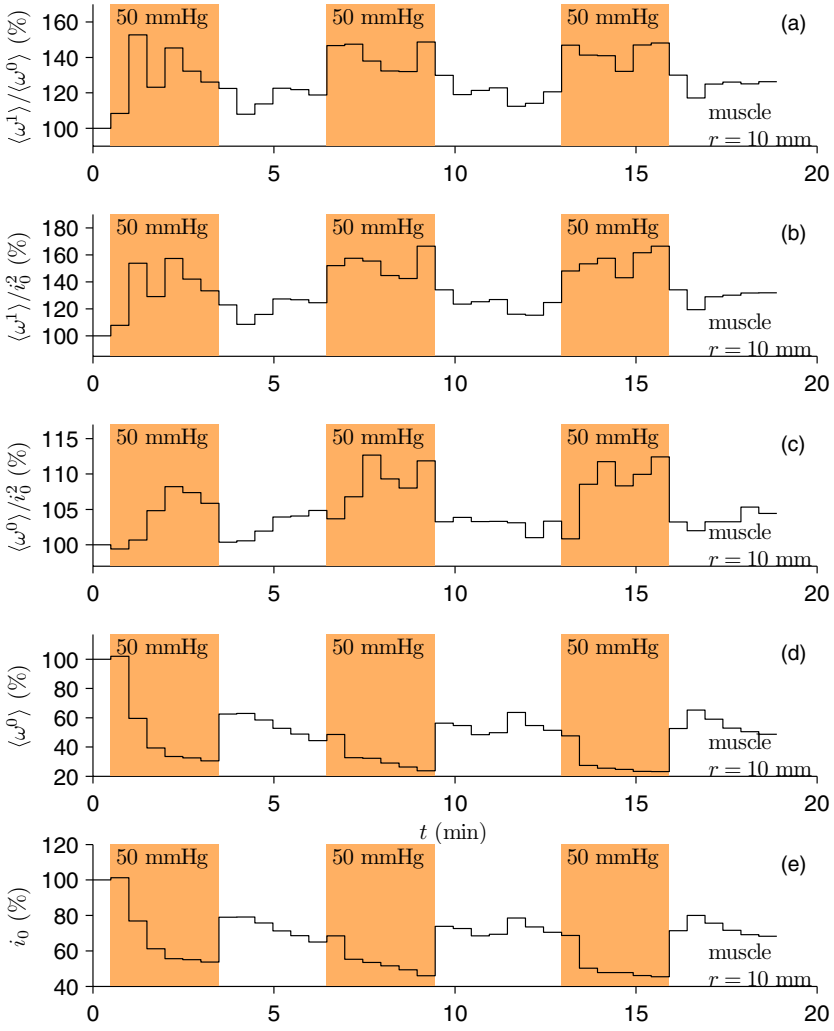

Figure 6. Muscle parameters assessed with interoptode spacing of 10 mm during three cycles of venous occlusion (orange region) at 50 mmHg. (a) First-moment divided by the zero-moment, $\langle\omega^1\rangle/\langle\omega^0\rangle$ (blood speed), of the power spectrum of the photo-electric current as a function of time, t. The $\langle\omega^1\rangle/\langle\omega^0\rangle$ values are normalized to 100% at time 0; (b–e) are the same as (a) but for $\langle\omega^1\rangle/i_0^2$ (blood perfusion), $\langle\omega^0\rangle/i_0^2$ (blood volume) i_0 and $\langle\omega^0\rangle$ (un-normalized blood volume), and where i_0 is the mean value of the photo-electric current (detected mean light intensity). The parameter r is the interoptode distance. The abscissa units are the same for the five panels.

periods suggests that the quantity of blood present in the region of interest increases (decrease in i_0), but that the number of randomly moving red blood cells present in this volume is small (i.e. small $\langle\omega^0\rangle/i_0^2$ values). This increase in blood volume is typically due to the cuff slightly squeezing the blood into the measured region of interest. To close this section, one can finally note again that during the arterial occlusion the parameters $\langle\omega^0\rangle/i_0^2$ (figure 7(c)) and $\langle\omega^0\rangle$ (figure 7(d)) go in the same direction as predicted by the Monte Carlo simulations, i.e. both decrease when the number of moving particles drastically diminishes due to the ischaemia (figures 4 and 5, markers with green edge).

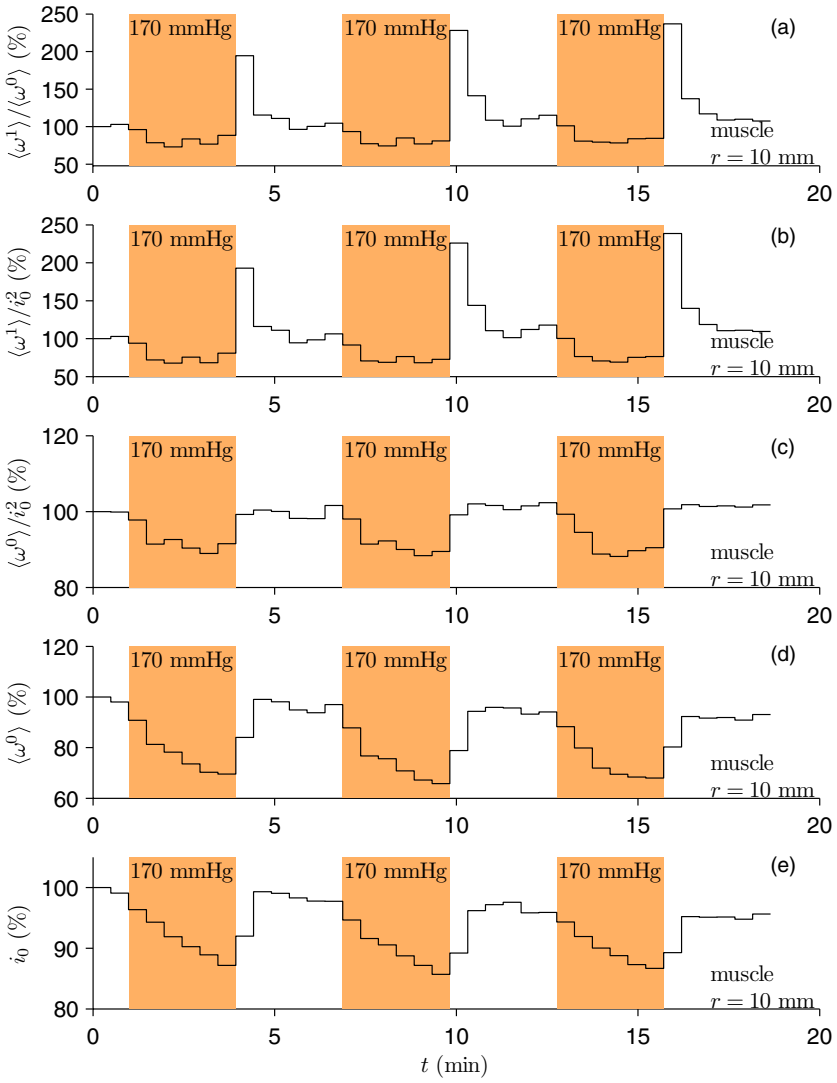

Figure 7. Muscle parameters assessed with interoptode spacing of 10 mm during three cycles of arterial occlusion (orange region) at 170 mmHg. The parameters are the same as in figure 6.

3.3. Experimental LDF tests: tibia

Figures 8–10 refer to measurements performed on bone (tibia diaphysis) and had the aim to check whether it is possible to monitor the LDF parameters at $r = 10$ mm and $r = 25$ mm during the same physiological manoeuvres previously applied to the muscle. We can reasonably suppose that for $r = 10$ mm the investigated region corresponds to the bone cortex and for $r = 25$ mm the light reaches mainly the bone marrow. In fact, near-infrared light can easily travel through the bone as it does for other tissues and it is largely used to perform studies on human brain. By exploiting this optical property, non-LDF studies aimed to directly investigate bone/marrow (Binzoni and Van De Ville 2011) have been performed. Recent work by Aziz *et al* (2010) also reports data in accordance with our findings. However,

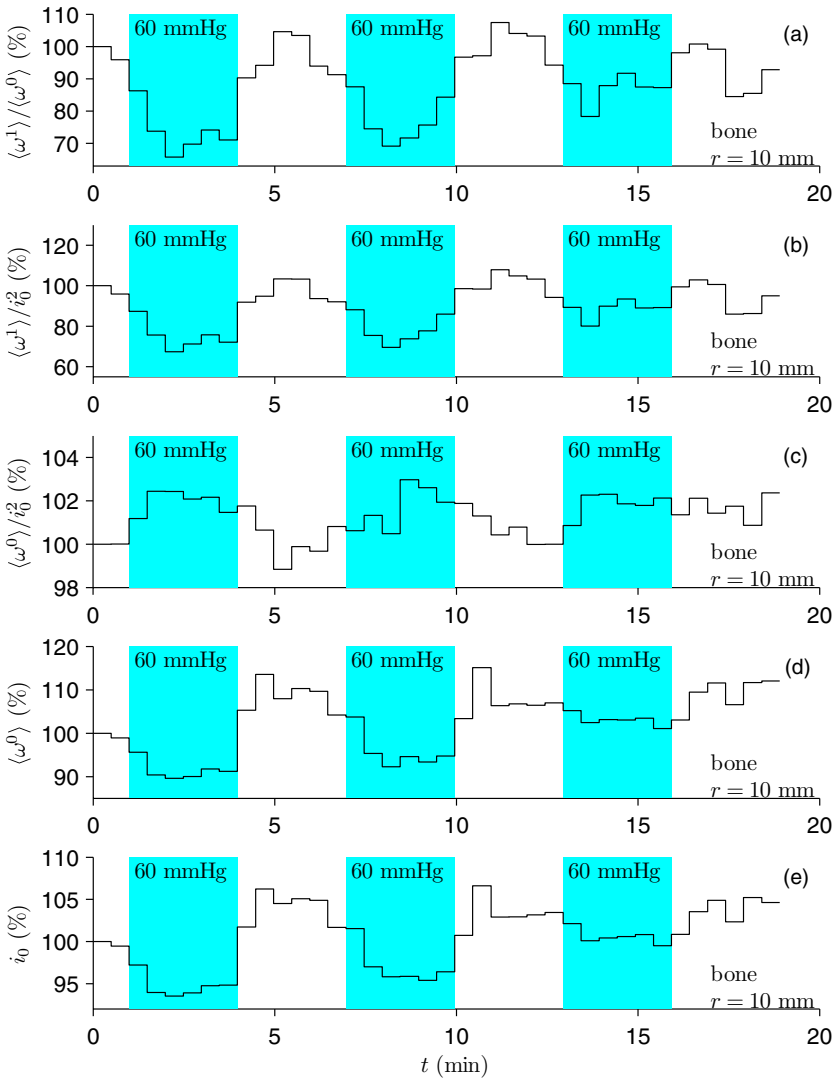

Figure 8. Bone parameters assessed with interoptode spacing of 10 mm during three cycles of venous occlusion (blue region) at 60 mmHg. The parameters are the same as in figure 6.

it is clear that future investigations better exploring light transport in bone, analogous to those performed by Meglinsky and Matcher (2001) for the human skin, will certainly be useful.

In figure 8, the venous occlusion protocol has been applied to the tibia ($r = 10$ mm). In opposition to the results obtained for the muscle (figure 6), in bone the mean blood speed, $\langle\omega^1\rangle/\langle\omega^0\rangle$, and the blood perfusion, $\langle\omega^1\rangle/i_0^2$, decrease during the occlusion (figures 8(a) and (b)). This probably means a different redistribution of blood flow during the venous occlusion between muscle and bone. However, as expected from the venous occlusion manoeuvre, the blood volume, $\langle\omega^0\rangle/i_0^2$ (and related parameters), tends to increase (figure 8(c)). Note that even this time $\langle\omega^0\rangle/i_0^2$ (figure 8(c)) and $\langle\omega^0\rangle$ (figure 8(d)) change by following opposite

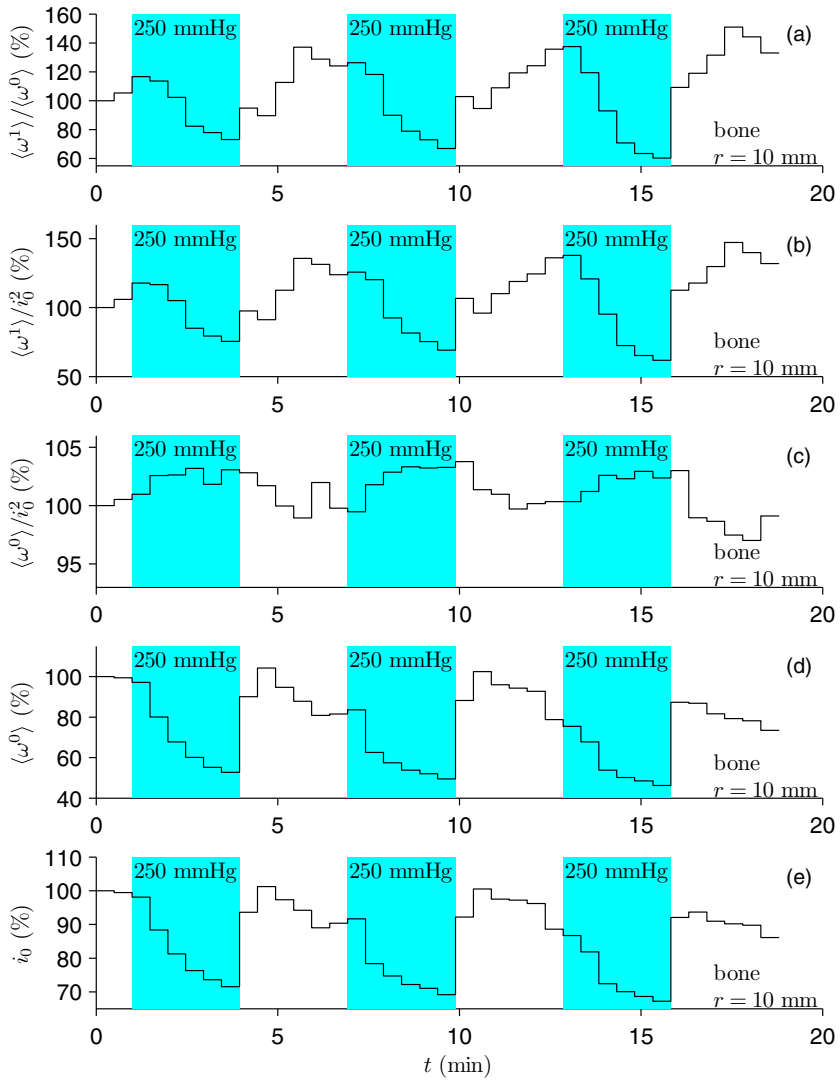

Figure 9. Bone parameters assessed with interoptode spacing of 10 mm during three cycles of arterial occlusion (blue region) at 250 mmHg. The parameters are the same as in figure 6.

directions. Note also the decrease in the amplitude of response of all the parameters to the venous occlusion manoeuvres over time, a distinctive feature of bone tissue compared to muscle.

In figure 9, the arterial occlusion protocol has been applied to the tibia ($r = 10$ mm). The rate at which the tissue mean blood speed, $\langle\omega^1\rangle/\langle\omega^0\rangle$, and the tissue blood perfusion, $\langle\omega^1\rangle/i_0^2$, reach the lowest value during the arterial occlusion is particularly slow. This demonstrates a slow redistribution of blood volume in the bone during the occlusion (i.e. the blood takes a while before its translational movement stops). This transient period may correspond to the fluid redistribution and vasomotion phase previously described by Kernick *et al* (1999) at small interoptode spacing. In the same manner, the rate at which the tissue mean blood speed, $\langle\omega^1\rangle/\langle\omega^0\rangle$, and the tissue blood perfusion, $\langle\omega^1\rangle/i_0^2$, recover after the cuff pressure

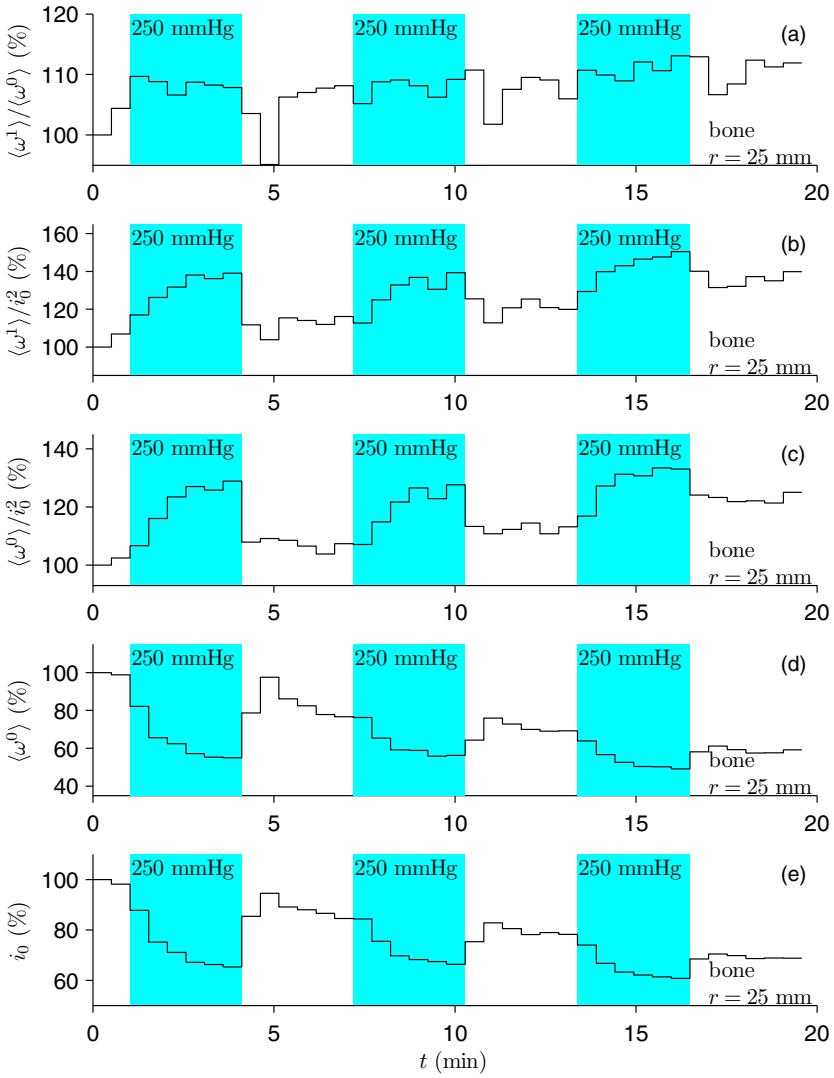

Figure 10. Bone/bone marrow parameters assessed with interoptode spacing of 25 mm during three cycles of arterial occlusion (blue region) at 250 mmHg. The parameters are the same as in figure 6.

release (figures 9(a) and (b)) is also a lot slower than that in muscle (figures 7(a) and (b)). A small increase in tissue blood volume, $\langle\omega^0\rangle/i_0^2$, is also manifest (figure 9(c)). This can be linked to the continuous movement of blood due to the slow blood volume redistribution and accumulation during the occlusion periods. Of course, another possibility is that 250 mmHg are not sufficient to completely stop tissue blood flow in bone. This topic is another matter for future studies.

The venous occlusion protocol applied to bone for $r = 25$ mm did not show significative changes in the LDF parameters; for this reason the data are not reported here. Probably, the effect of the venous occlusion was absorbed by the surrounding skeletal muscle but not in the bone marrow. On the contrary, the arterial occlusion protocol ($r = 25$ mm) was able to

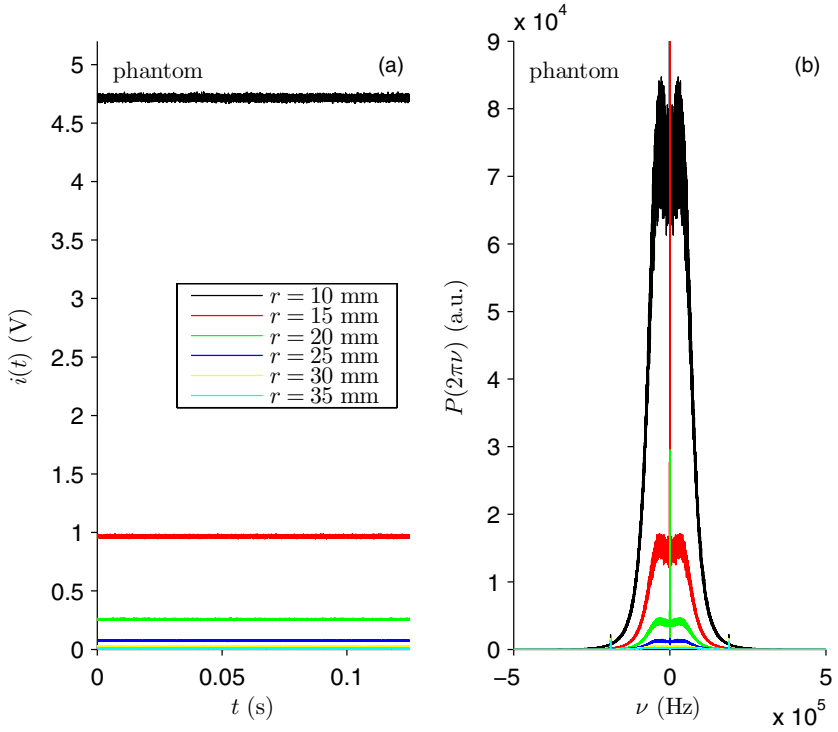

Figure 11. (a) Photo-electric current, $i(t)$, as a function of time, t, for different interoptode distances, r, measured on a tissue phantom. The phantom parameters were $\mu_a = 0.02$ mm^{-1} $\mu_s' = 0.5$ mm^{-1} at 815 nm; (b) Power density spectrum (mean of 600 power spectra), $P(2\pi\nu)$, of the corresponding $i(t)$ (see colours). The parameter ν is the frequency.

modulate the LDF parameters. In figure 10, it is possible to see that i_0 slowly decreases during the ischaemic periods and thus this is the witness of an increase of blood volume. For this reason, $\langle\omega^0\rangle/i_0^2$ never decreases to the biological zero values because there is always some moving blood during the occlusion. The increase in bone marrow blood volume during arterial occlusion confirms previous observations (made at $r = 30$ mm) by Binzoni *et al* (2003a). This observation is compatible with the behaviour of the tissue blood perfusion, $\langle\omega^1\rangle/i_0^2$, that increases during the blood volume increase.

4. Discussion and conclusions

4.1. Technical comments on LDF measurements

4.1.1. The power spectral density baseline. We first highlight a particular technical property of the APD module that, if neglected by using a too low sample rate of the photoelectric current (even if enough to cover the laser-Doppler frequencies), could introduce in some cases large errors in the estimation of $\langle\omega^0\rangle$ and $\langle\omega^1\rangle$. This problem becomes important for LDF at large interoptode spacing.

To intuitively explain the problem in figure 11 a series of measurements obtained with the present LDF instrument on an optical tissue phantom built at the University College of London (Firbank *et al* 1995) are reported. This homogeneous phantom reproduces the optical

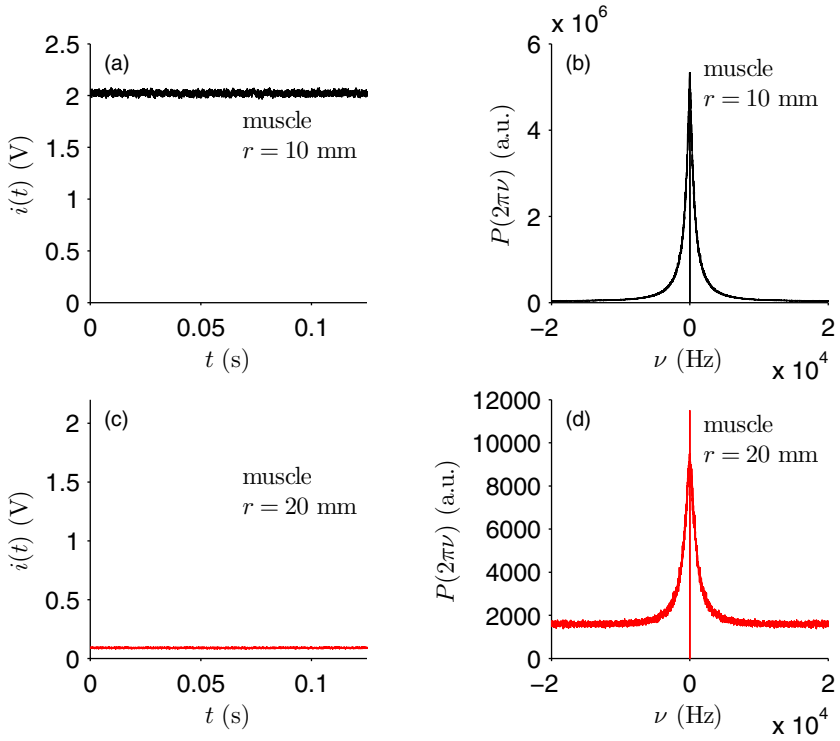

Figure 12. (a) Photo-electric current, $i(t)$, as a function of time, t, for the forearm. The parameter r is the interoptode distance. (b) Power density spectrum (mean of 600 power spectra), $P(2\pi\nu)$, of the correspondent $i(t)$ (see colours). The parameter ν is the frequency. The baseline has a mean value of 39 602 au (difficult to observe due to the size of the spectrum). (c) and (d) same as (a) and (b) but with a different r. The baseline in (d) has a mean value of 1596 au.

properties of a biological tissue but without 'blood flow'. The aim was to monitor the LDF signal in the case where the photons do not interact with moving scatterers and observe the measured $i(t)$ and $P(2\pi\nu)$.

Figure 11 reveals that when we perform measurements at different r, we obtain a series of $i(t)$ for which i_0 roughly varies logarithmically as a function of r (figure 11(a)). The power spectrum density, $P(2\pi\nu)$, for each measured $i(t)$ (figure 11(b)) has an amplitude that varies as a function of i_0. Actually, the real $P(2\pi\nu)$ generated by the APD is a flat baseline; however, the APD module electronics contain a characteristic bandpass filter which gives rise to the shape of $P(2\pi\nu)$. The important point here is that the APD module has been built to have a constant $P(2\pi\nu)$ ('flat') in the ν interval that will contain the Doppler shifts observed during real measurements on biological tissues (e.g. $[2 \times 10^{-4}, 2 \times 10^4]$ Hz).

Figure 12 shows the practical consequence of the above 'baseline effect' on two measurements performed on the forearm for two different r. Figures 12(a) and (c) report $i(t)$ and figures 12(b) and (d) the corresponding $P(2\pi\nu)$. If the detected i_0 is large (figure 12(a)), then the 'baseline' is negligible compared to the Doppler spectrum, and thus this effect can safely be neglected (figure 12(b)). However, if the signal is poor (for small i_0), then the amplitude of the 'baseline' becomes non-negligible compared to the wanted spectrum (figure 12(b)). In this case, the 'baseline' will introduce very large errors when computing $\langle\omega^0\rangle$ and $\langle\omega^1\rangle$ (see equation (1)). These observations also explain the necessity to sample $i(t)$

at high rate (1 MHz), which is largely above the observed Doppler frequencies and eliminates the risk of aliasing artifacts due to folding and superposition of the baseline spectrum over the Doppler spectrum of interest.

In conclusion, it is necessary to subtract adaptively the 'baseline' from each power density spectrum over the integration interval before computing $\langle\omega^0\rangle$ and $\langle\omega^1\rangle$, which is the procedure that was followed on the experimental data of the present contribution.

4.1.2. Blood oxygen saturation of tissue and LDF signals. In the experimental part of the present contribution we have used a $\lambda = 785$ nm CW laser. This wavelength is not at the isosbestic point for the haemoglobin ($\lambda \approx 805$ nm) and thus a physio-/pathological induced change in blood oxygen saturation (SO_2) also changes in principle the optical properties (μ_a) of the investigated tissue. A variation in μ_a theoretically induces also a change in the region of interest visited by the light (Kohl *et al* 1998), and the photons will travel on different paths depending on the μ_a values. Intuitively, photons travelling on longer paths will accumulate more Doppler shifts and give contributions to higher ν on the spectrum. This may potentially create a measurement artifact when computing $\langle\omega^0\rangle$ and $\langle\omega^1\rangle$ from these spectra (e.g. the detection of a blood perfusion change that does not exist in reality).

Obviously, the best solution would be to use $\lambda \approx 805$ nm that completely eliminates the problem. However, the interest here is that it is in principle possible to imagine to combine two Doppler signals at different λ and to exploit the obtained $i(t)$ to calculate by standard NIRS methods the time-variations in oxy-(HbO_2) and deoxy-haemoglobin (Hb) concentration. This could allow LDF instrumentation to generate extremely valuable new physiological information just by doubling its basic components.

Fortunately, an estimation of the influence of SO_2 on μ_a (not presented here for reasons of space) shows that the error on μ_a is in general smaller than ~2% at 785 nm and thus the influence of SO_2 changes on $\langle\omega^0\rangle$ and $\langle\omega^1\rangle$ can be neglected. Our estimation is in agreement with previous findings by Kohl *et al* (1998) where they demonstrated that the variation of the differential pathlength factor of a tissue as a function of SO_2 may be considered negligible if $\lambda > 790$ nm.

In conclusion, the above estimation shows that lasers with a λ different from the isosbestic point can be reasonably used in LDF at large optode spacing if, for example, multiple wavelength measurements are needed.

4.2. Monte Carlo simulations

In the present contribution it has been shown by exploiting the results of 32 days of Monte Carlo simulations that $\langle\omega^0\rangle/i_0^2$ and $\langle\omega^1\rangle/i_0^2$ measured at large r can still be linearly related to tissue blood volume and tissue blood flow as it is classically observed for small r. The sensitivity of $\langle\omega^0\rangle/i_0^2$ for a change in P_{move}, at $r \geqslant 10$ mm, is smaller (~5%) than for $r = 0.5$ mm, but it can still be detected experimentally. The more reliable parameter appears to be $\langle\omega^1\rangle/\langle\omega^0\rangle$ (mean blood speed). In fact, $\langle\omega^1\rangle/\langle\omega^0\rangle$ is the only parameter not affected by the value of μ_s'. It has also been shown that in the case of an arterial occlusion (very small P_{move} value, independent from μ_a), the parameter $\langle\omega^0\rangle/i_0^2$ reaches its lowest values. This level, during an ischaemia, is classically called the 'biological zero' (Tenland *et al* 1983) condition. As expected, for a chosen set of optical and physiological parameters, the 'biological zero' value for $\langle\omega^0\rangle/i_0^2$ is 'proportionally' higher at $r \geqslant 10$ mm compared to $r = 0.5$ mm. This is mainly explained by the fact that at $r \geqslant 10$ mm the region of interest visited by the photons is larger than that at $r = 0.5$ mm, and thus the photons have the possibility of making more interactions with red blood cells before reaching the photo-detector, therefore increasing the

'area' under the power spectrum. It must be noted that *in vivo* other scatterers (e.g. large intersticial molecules) may participate to the 'biological zero' (Kernick *et al* 1999), but this does not change the bases of the present explanation. The parameter i_0 also decreases for increasing r and thus participates to amplify the effect. This is not shown explicitly in the figure, but the increase in the 'biological zero' value (proportionally) for increasing r remains valid also for the non-normalized $\langle\omega^0\rangle$.

One important conclusion of the present simulations is that LDF at large r allows the same physiological signals to be detected as in classical LDF. This permits us to build a very simple and cost effective LDF instrument that does not need the utilization of autocorrelators or single-photon detectors, and this is what has been done for the experimental part of this work.

4.3. Experimental LDF tests: forearm

The batch of experimental LDF tests performed on a human forearm at $r = 10$ mm has allowed us to effectively monitor known behaviour of tissue blood perfusion or blood volume when the muscle is submitted to physiological challenges such as in the case of venous or arterial occlusions[5]. For example, the expected volume increase during venous occlusion or the post-ischaemic hyperaemia were well detected by the LDF instrument. The experimental tests have also shown that the real measurements behave as predicted by Monte Carlo simulations. In particular, the measurements reproduce the special predicted behaviour of the non-normalized $\langle\omega^0\rangle$ at large r (i.e. decreasing $\langle\omega^0\rangle$ when $\langle\omega^0\rangle/i_0^2$ increases).

4.4. Experimental LDF tests: tibia

To the best of our knowledge, these are the first LDF measurements performed non-invasively on human bone/bone marrow at large interoptode spacing. In the present contribution, we have used two different distances to access different tissue depth; however, it is clear that in the future more detailed studies at various r and relative Monte Carlo simulations will be necessary to be performed to better understand the behaviour of the light inside a human tibia diaphysis. This will allow us to better define the exact regions sampled by the LDF technique. In this work, it has been possible to show that changes in blood flow and blood volume are indeed detectable in the human tibia, in a continuous manner, and non-invasively. Even if the technique can certainly be improved in terms of spatial localization and time resolution it already appears a very promising result allowing unique measurements to be performed *in vivo* on human bone. In fact, one must realize that other non-invasive techniques such as those based on ultrasound cannot be utilized in bone, because the waves do not penetrate the tissue. The remaining techniques that do not interfere too much with the studied physiological system are based on ionizing radiation which limits the number and frequency of measurements *in vivo* and unlike LDF does not allow continuous measurements in time. Moreover, in this case to detect a flow it is necessary to inject contrast agents and this does not allow continuous measurement in time.

4.5. Discussion and conclusions

We have shown that LDF at large r allows us to monitor bone/bone marrow blood perfusion in humans (tibia diaphysis). As in classical LDF, the measurements do not give absolute values;

[5] Similar to other near-infrared measurement techniques, LDF does not allow us to distinguish between the arterial and venous side, but gives only an overall mean value of the measured parameter.

however, the technique has a series of unique advantages, such as the non-invasiveness or the possibility of monitoring signals in real-time for very long and repeated periods, that will permit future studies of a new kind on neuro-vascular control in bone/bone marrow.

The non-invasiveness of LDF is an extremely important advantage because the measurements do not influence the studied physiological system. In fact, as we have already mentioned in the introduction, blood flow regulation in human bone/bone marrow is controlled by the autonomic (sympathetic) nervous system (Brookes and Revell 1998). The autonomic system, and as a consequence tissue blood flow perfusion, may be strongly influenced for example by mental challenges such as stress (Blair *et al* 1959, Hamer *et al* 2006) or hypnosis (Perry 1980), mechanisms that have implications on important psychobiological disease pathways. It is clear that if one wants to better understand the role of these very particular mechanisms in the control of human bone/bone marrow circulation it is essential not to perturb the system/subject with the measurement technique, and LDF seems to be the ideal approach. This is why even if LDF at large interoptode spacing appears to be at this preliminary stage only a rudimentary approach, it actually already allows us to imagine experimental protocols that are not feasible with any other techniques.

Another advantage of LDF at large r is the possibility of continuously monitoring the parameters related to tissue blood perfusion. A typical example may be perfectly well represented by the experimental tests performed in this work on the human tibia diaphysis. Probably, there are no other techniques, even invasive, allowing the measurement of bone/bone marrow blood volume or speed with a sampling time of 29 s and during 20 min. In this sense, we have no limits on the duration of the measurement and, if necessary, the time resolution can also easily be shortened by some simple technical improvements, such as adapting the laser power or better by using multiple (cost effective) APD detectors. These technical improvements should also allow us to see if fast blood pulsations and vasomotion that are usually observed in other tissues are also observable in bone/bone marrow.

We also note that invasive techniques that relay on radio-tracers (e.g. Tothill 1984, Iida *et al* 1999) are complementary to LDF. The advantage of these techniques, such as PET, is their capability to obtain more precise spatial information and, in particular, to generate absolute values. Therefore, these approaches may be used in the future to 'calibrate' LDF signals for particular protocols.

In conclusion, we hope that the present contribution will stimulate new studies on the neuro-vascular control in human bone/bone marrow (e.g. by using hypnosis, suitable physiological manipulations or pharmacological means), a domain that has always been extremely difficult to investigate experimentally.

Acknowledgments

The authors kindly thank Professor Alwin Kienle for the useful information and explanations concerning the model represented by equation (4).

References

Aziz S M, Khambatta F, Vaithianathan T, Thomas J C, Clark J M and Marshall R 2010 A near infrared instrument to monitor relative hemoglobin concentrations of human bone tissue *in vitro* and *in vivo* *Rev. Sci. Instrum.* **81** 043111-1–7

Binzoni T, Bianchi S, Fasel J H, Bounameaux H, Hiltbrand E and Delpy D T 2002 Human tibia bone marrow blood perfusion by non-invasive near infrared spectroscopy: a new tool for studies on microgravity *J. Gravit. Physiol.* **9** P183–4

Binzoni T, Leung T S, Boggett D and Delpy D 2003 Non-invasive laser Doppler perfusion measurements of large tissue volumes and human skeletal muscle blood RMS velocity *Phys. Med. Biol.* **48** 2527–49

Binzoni T, Leung T S, Courvoisier C, Giust R, Tribillon G, Gharbi T and Delpy D T 2006 Blood volume and haemoglobin oxygen content changes in human bone marrow during orthostatic stress *J. Physiol. Anthropol.* **25** 1–6

Binzoni T, Leung T, Hollis V, Bianchi S, Fasel J H, Bounameaux H, Hiltbrand E and Delpy D 2003a Human tibia bone marrow: defining a model for the study of haemodynamics as a function of age by near infrared spectroscopy *J. Physiol. Anthropol. Appl. Human. Sci.* **22** 211–8

Binzoni T, Leung T S, Seghier M L and Delpy D T 2004 Translational and Brownian motion in laser-Doppler flowmetry of large tissue volumes *Phys. Med. Biol.* **49** 5445–58

Binzoni T, Leung TS and Van De Ville D 2009 The photo-electric current in laser-Doppler flowmetry by Monte Carlo simulations *Phys. Med. Biol.* **54** N303–18

Binzoni T and Van De Ville D 2008 Full-field laser-Doppler imaging and its physiological significance for tissue blood perfusion *Phys. Med. Biol.* **53** 6673–94

Binzoni T and Van De Ville D 2011 Non-invasive probing of the neuro-vascular system in human bone/bone-marrow using near-infrared light *J. Innov. Opt. Health Sci.* **4** 183–9

Blair D A, Glover D E, Greenfield A D and Roddie I C 1959 Excitation of cholinergic vasodilator nerves to human skeletal muscles during emotional stress *J. Physiol.* **148** 633–47

Bonner R F and Nossal R 1981 Model for laser Doppler measurements of blood flow in tissue *Appl. Opt.* **20** 2097–107

Brookes M and Revell W J 1998 *Blood Supply of Bone: Scientific Aspects* (London: Springer)

Chenu C 2001 Innervation de l'os *médecine/sciences* **17** 1276–80

De Blasi R A, Ferrari M, Natali A, Conti G, Mega A and Gasparetto A 1994 Noninvasive measurement of forearm blood flow and oxygen consumption by near-infrared spectroscopy *J. Appl. Physiol.* **76** 1388–93

Firbank M, Oda M and Delpy D T 1995 An improved design for a stable and reproducible phantom material for use in near-infrared spectroscopy and imaging *Phys. Med. Biol.* **40** 955–61

Hamer M, Boutcher Y N, Park Y and Boutcher S H 2006 Reproducibility of skeletal muscle vasodilatation responses to Stroop mental challenge over repeated sessions *Biol. Psychol.* **73** 186–9

Iida S, Harada Y, Ikenoue S and Moriya H 1999 Measurement of bone marrow blood volume in the knee by positron emission tomography *J. Orthop. Sci.* **4** 216–22

Kernick D P, Tooke J E and Shore A C 1999 The biological zero signal in laser Doppler fluximetry—origins and practical implications *Pflugers Arch.* **437** 624–31

Kienle A 2001 Non-invasive determination of muscle blood flow in the extremities from laser Doppler spectra *Phys. Med. Biol.* **46** 1231–44

Klein-Nulend J, Bacabac R G and Mullender M G 2005 Mechanobiology of bone tissue *Pathol. Biol. (Paris)* **53** 576–80

Kohl M, Nolte C, Heekeren H R, Horst S, Scholz U, Obrig H and Villringer A 1998 Determination of the wavelength dependence of the differential pathlength factor from near-infrared pulse signals *Phys. Med. Biol.* **43** 1771–82

Meglinsky I V and Matcher S J 2001 Modelling the sampling volume for skin blood oxygenation measurements *Med. Biol. Eng. Comput.* **39** 44–50

McCarthy I 2006 The physiology of bone blood flow: a review *J. Bone Joint Surg. Am.* **88** 4–9

Näslund J, Pettersson J, Lundeberg T, Linnarsson D and Lindberg L G 2006 Non-invasive continuous estimation of blood flow changes in human patellar bone *Med. Biol. Eng. Comput.* **44** 501–9

Perry B J 1980 Control of physiological phenomena via hypnosis with special reference to contraception *Aust. J. Clin. Hypnother.* **1** 73–7

Tenland T, Salerud E G, Nilsson G E and Oberg P A 1983 Spatial and temporal variations in human skin blood flow *Int. J. Microcirc. Clin. Exp.* **2** 81–90

Tothill P 1984 Bone blood flow measurement *J. Biomed Eng.* **6** 251–5

Tuncali B, Karci A, Tuncali B E, Mavioglu O, Ozkan M, Bacakoglu A K, Baydur H, Ekin A and Elar Z 2006 A new method for estimating arterial occlusion pressure in optimizing pneumatic tourniquet inflation pressure *Anesth. Analg.* **102** 1752–7